

UC San Diego

UC San Diego Previously Published Works

Title

Characterizing Breast Lesions Using Quantitative Parametric 3D Subharmonic Imaging: A Multicenter Study

Permalink

<https://escholarship.org/uc/item/6892k2pd>

Journal

Academic Radiology, 27(8)

ISSN

1076-6332

Authors

Sridharan, Anush
Eisenbrey, John R
Stanczak, Maria
[et al.](#)

Publication Date

2020-08-01

DOI

10.1016/j.acra.2019.10.029

Peer reviewed



Published in final edited form as:

Acad Radiol. 2020 August ; 27(8): 1065–1074. doi:10.1016/j.acra.2019.10.029.

Characterizing breast lesions using quantitative parametric 3D subharmonic imaging: A multi-center study

Anush Sridharan, PhD^{1,2}, John R. Eisenbrey, PhD¹, Maria Stanczak, MS¹, Priscilla Machado, MD¹, Daniel A. Merton, RDMS¹, Annina Wilkes, MD¹, Alexander Sevrukov, MD¹, Haydee Ojeda-Fournier, MD³, Robert F. Mattrey, MD³, Kirk Wallace, PhD⁴, Flemming Forsberg, PhD¹

¹Department of Radiology, Thomas Jefferson University, Philadelphia, PA 19107, USA

²Department of Electrical and Computer Engineering, Drexel University, Philadelphia, PA 19104, USA

³Department of Radiology, University of California, San Diego, CA 92103, USA

⁴GE Global Research, Niskayuna, NY 12309, USA

Abstract

Rationale and Objectives—Breast cancer is the leading type of cancer among women.

Visualization and characterization of breast lesions based on vascularity kinetics was evaluated using three-dimensional (3D) contrast-enhanced ultrasound imaging in a clinical study.

Materials and Methods—Breast lesions (n = 219) were imaged using power Doppler imaging (PDI), 3D contrast-enhanced harmonic imaging (HI) and 3D contrast-enhanced subharmonic imaging (SHI) with a modified Logiq 9 ultrasound scanner using a 4D10L transducer. Quantitative metrics of vascularity derived from 3D parametric volumes (based on contrast perfusion; PER and area under the curve; AUC) were generated by off-line processing of contrast wash-in and wash-out. Diagnostic accuracy of these quantitative vascular parameters was assessed with biopsy results as the reference standard.

Results—Vascularity was observed with PDI in 93 lesions (69 benign and 24 malignant), 3D HI in 8 lesions (5 benign and 3 malignant) and 3D SHI in 83 lesions (58 benign and 25 malignant). Diagnostic accuracy for vascular heterogeneity, PER and AUC ranged from 0.52 to 0.75, while the best logistical regression model (vascular heterogeneity ratio, central PER and central AUC) reached 0.90.

Conclusion—3D SHI successfully detects contrast agent flow in breast lesions and characterization of these lesions based on quantitative measures of vascular heterogeneity and 3D parametric volumes is promising.

Corresponding Author: Flemming Forsberg, PhD, FAIUM, FAIMBE, Professor of Radiology, Department of Radiology, 763H Main Building, Thomas Jefferson University, 132 South 10th Street, Philadelphia, PA 19107, USA, Tel: +1-215-955-4870, flemming.forsberg@jefferson.edu.

Publisher's Disclaimer: This is a PDF file of an unedited manuscript that has been accepted for publication. As a service to our customers we are providing this early version of the manuscript. The manuscript will undergo copyediting, typesetting, and review of the resulting proof before it is published in its final form. Please note that during the production process errors may be discovered which could affect the content, and all legal disclaimers that apply to the journal pertain.

Keywords

breast cancer; contrast-enhanced ultrasound; subharmonic imaging; ultrasound contrast agents

Introduction

In 2018 an estimated 266,120 new cases of breast cancer were reported in the United States¹. Among females, breast cancer constitutes 30% of all of cancer types making it the leading type of cancer in women. Despite significant advancements in diagnosis and treatments, breast cancer is still the second leading cause of cancer-related deaths, accounting for 14% of all cancer-related deaths among females in the United States¹. Earlier detection of breast cancer can yield better treatment outcomes. Currently, mammography is the primary imaging modality for breast cancer screening in the United States.

Approximately, 90% of all screening mammograms performed annually show no evidence of cancer. However, of those with abnormal findings and receive a recommendation for biopsy approximately 80% are benign^{2,3}. Furthermore, when considering different age groups, mammography performed worse as a screening tool in women 40 years or younger (sensitivity 76.5% and specificity 87.1%) compared to older women (50-54 years; sensitivity 82.6% and specificity 90.4% or 70-74 years; sensitivity 86.3% and specificity 93.3%)^{4,5}. Additionally in these younger women, both the screening and diagnostic specificity are reduced with increasing breast density⁴.

Malignant lesions tend to have abnormal, chaotic and leaky vasculature as a result of rapid unstructured formation of new vessels. Termed “angiogenesis,” a tumor must continuously stimulate the growth of new capillary blood vessels for the tumor itself to grow beyond 2-3 mm^{3,6-8}. Characterizing this vascularity may provide vital information for differentiating malignant from benign lesions. The high number of non-malignant findings after biopsy and low specificity in younger women is a cause for concern. There is a clear need for an imaging modality (as an adjunct to mammography or as a stand-alone modality) that is able to improve characterization of breast lesions at an early stage, while simultaneously being cost-effective and patient-friendly.

Ultrasound imaging offers the capacity to visualize breast anatomy and vascular structures using Doppler techniques. Conventional ultrasound techniques (i.e., grayscale and Doppler imaging) have been studied as a supplement to mammography for examining breast lesions with mixed results, especially since in the early stages of tumor growth angiogenic neovessels are small (<100 μm) and have slow blood flow (<1 mm/s)^{3,9-13}. Advancements in ultrasound imaging technology in the last decade has provided the capability to image smaller structures such as lesions and their associated microvasculature¹⁴⁻¹⁶. Although these modes are promising, they are susceptible to motion-induced noise artifacts and breathing artifacts.

Alternatively, another technique for imaging vascularity using ultrasound involves the use of ultrasound contrast agents (UCAs), which are gas-filled microbubbles stabilized with an outer shell. These microbubbles range in diameter from 1-8 μm allowing them to circulate as intravascular agents without extravasation from the vascular space¹⁷⁻²⁴. UCAs can enhance

signals from vascular structures in the body by up to 30 dB. However, since there is signal also being generated from tissue, delineation of lesion vascularity can be challenging; especially the microvascular structures of the lesion. With sufficient acoustic excitation and correct transmit frequency (f_0), UCAs are able to produce nonlinear oscillations that span a wide range of frequency components from the subharmonic ($f_0/2$) to higher harmonics ($n \cdot f_0$). By selectively receiving a specific harmonic, it is possible to improve UCA detection by substantially reducing the mostly linear echoes from tissue. Generation of the subharmonic frequency component is specific to the UCA. Most commercial ultrasound scanners employ excitation/filtering techniques focusing on the second harmonic (so-called harmonic imaging; HI). However, HI suffers from low UCA signal-to-tissue ratio, because of second harmonic generation in the surrounding tissue²⁵. Imaging at the subharmonic frequency (so-called subharmonic imaging; SHI) allows for improved UCA signal-to-tissue ratios by providing near complete tissue suppression. The use of SHI has been extensively studied and validated independently by various groups^{18,26–31}. The first human studies of SHI for imaging breast lesions were performed comparing its performance to regular grayscale, Doppler and mammography with histopathology as the reference standard³². Results from that pilot study of 14 women showed that SHI had the highest accuracy with a receiver operating characteristic (ROC) curve area under the curve (A_z) of 0.78. Moreover, when combined with a dynamic cumulative maximum intensity technique (CMI) this A_z improved to 0.90³³.

Based on these encouraging results, the use of quantitative biomarkers derived from contrast-enhanced 3D HI and 3D SHI for characterization of breast lesions was investigated in a larger cohort of patients.

Materials and Methods

This multi-center clinical study was approved by the Institutional Review Boards of Thomas Jefferson University (TJU) and University of California–San Diego (UCSD). The study was conducted between January, 2011 and December, 2015. Data analysis was completed by June, 2017. The study was compliant with the Health Insurance Portability and Accountability Act. Furthermore, this study was carried out under an FDA approved IND (no 112,241) and in accordance with [ClinicalTrials.gov](https://www.clinicaltrials.gov) registration (NCT 01490892). Women (21 years or older) who were scheduled for a breast biopsy based on their mammography and/or grayscale ultrasound examinations conducted as part of their clinical standard of care were enrolled in this study after providing written informed consent and meeting all inclusion criteria and exclusion criteria (see Appendix).

All ultrasound imaging was performed on a commercially available Logiq 9 scanner (GE Healthcare, Waukesha, WI) equipped with a 4D10L probe that was modified to perform 3D HI and 3D SHI.³¹ For 3D HI, the transmit frequency was set at 5.0 MHz (using a 2-cycle transmit pulse) and receiving at 10.0 MHz (bandpass filtered). For 3D SHI, transmit frequency was 5.8 MHz (using a 4-cycle transmit pulse) and receiving at 2.9 MHz (equalization filtered). Pulse inversion (summing 2 consecutive signals 180° out of phase) was implemented for both contrast modes to reduce (or eliminate) any remaining linear background signals. The mechanical index (MI) at maximum transmit settings was measured

as 0.36 for 3D HI (peak negative pressure of 0.80 MPa) and 0.33 (peak negative pressure of 0.79 MPa) for 3D SHI using a 0.5 mm needle hydrophone (Precision Acoustics, Dorset, UK). Extensive *in vitro* and *in vivo* testing of the scanner modifications were conducted prior to the initiation of clinical evaluation³⁴.

The UCA used for this study was Definity™ (Lantheus Medical Imaging, N Billerica, MA)^{35,36}. This UCA consists of perflutren lipid microbubbles composed of octafluoropropane encapsulated in a lipid shell. After activation, the UCA has a mean diameter of 1.1-3.3 μm with approximately 1.2×10^{10} microbubbles per mL and around 1.3 mL of agent available in a single vial. The US transmit and receive frequencies for 3D HI and 3D SHI were optimized for use with Definity based on testing in previous studies^{34,37}.

Ultrasound Imaging

Prior to the clinically indicated biopsy, the location of the lesion was identified using 2D grayscale ultrasound and confirmed based on the available prior imaging. After localization, the lesion was measured along its longest axes on both transverse and sagittal planes using 2D grayscale ultrasound and measurements recorded. Next, baseline 2D grayscale and 2D power Doppler imaging (PDI) cine clips were acquired by manually sweeping across the entire lesion. Once all baseline images were acquired the patients were prepped for the contrast studies by placing an intravenous catheter (ideally 22 gauge or larger)³⁸ in a peripheral vein, typically the antecubital vein. The UCA Definity was activated using the Vialmix™ shaker (supplied by Lantheus Medical Imaging) and the required UCA bolus dosage was selected based on prior imaging experience by our group for HI (0.25 mL ± 10 mL saline flush) and SHI (20 μL/kg up to a maximum of 1.25 mL+ 10 mL saline flush)^{32,37}.

Prior to starting 3D volume acquisition, ultrasound imaging parameters such as image gain (dB), acoustic power/output (%), image depth (cm), focal position (cm), volume angle (degree), and image quality were selected to allow visualization of the entire lesion with good UCA signal-to-tissue contrast. The imaging parameters for 3D HI and 3D SHI were optimized based on previous *in vitro* and pre-clinical animal imaging studies to achieve the best contrast-to-tissue signal ratio^{34,37}. These studies provided a good starting point for the anticipated range of these parameters for clinical translation. Further optimization of imaging settings was performed during the initial clinical studies in this patient cohort. These imaging parameters were independently adjusted for the 3D contrast imaging modes to minimize the background tissue signals, while maintaining sufficient acoustic power/output to get a signal response from the microbubbles. 'Image quality' was a preset configurable option on the GE Logiq 9 scanner in the 3D contrast imaging modes that related to the line density of the rendered image. An increase in 'quality' equaled a higher line density, but the trade-off was a lower volume acquisition rate. The default volume angle was set to 19 degrees, which for smaller lesions (less than 1 cm³) meant volume acquisition rates were around 3 Hz. For larger lesions (greater than 3 cm³) the acquisition rate dropped to 1.1-1.6 Hz, due to the increase in the size of the lesion/imaging area. For contrast imaging, 3D HI volumes were acquired first. Volume acquisition was started simultaneously with the UCA bolus administration and continued until sufficient washout (dissipation) of the UCA was observed on the scanner display (typically around 60 s). After clearance of UCA and

return to baseline, approximately 10-15 minutes, the second UCA injection was administered and 3D SHI volumes collected similar to 3D HI acquisition procedure. In total, two still images of the lesion size measurements (along the sagittal and transverse planes), two cine clips of the 2D baseline grayscale and PDI sweeps across the lesion and two volumetric cine files containing the contrast-enhanced 3D HI and 3D SHI volumes, respectively, were acquired for each patient. Ultrasound scanning was performed by an experienced sonographer at each site.

Image Processing

Once the study was completed, images were transferred from the ultrasound scanner to a desktop computer for offline image processing and analysis. Custom image processing and analysis tools were built using MATLAB (2012a, The Mathworks Inc., Natick, MA) to perform the analysis as described in our previous work³¹. The lesions that demonstrated UCA flow were identified by a radiologist (with 10+ years of experience) in consensus with an ultrasound physicist using a proprietary software 4DView (GE Medical Systems, Zipf, Austria). This software allowed for volumetric visualization of the acquired 3D HI and 3D SHI images. Each of these volumes could be manipulated in a 3D space, segmented into individual 2D planes/slices and viewed along the time series of the acquisition thus, providing the radiologist a comprehensive tool for assessing the vascularity and its behavior across the entire lesion (see Figure 1A).

In cases that did demonstrate UCA flow, a region-of-interest (ROI) corresponding to the area of vascularity was localized in 4DView and the spatial coordinates of this ROI were projected through the entire 3D volume containing the (see Figure 1B) individual 2D slices extracted in MATLAB. Time intensity curves (TIC) based on the average image intensity within each ROI for all 2D slice across 3D volume were used to generate a single 3D TIC volume and specific time-points representative of the UCA flow within the ROI across the entire lesion were identified (Table 1).

Subsequently, the 3D TIC volumes were used to generate vascular heterogeneity maps (in the central, and peripheral zones/regions as well as a ratio of the two). The peripheral region was defined as the outer third of the entire tumor area including 2 mm around the lesion boundary and rest constituted the central regions. The 3D parametric volumes were based on perfusion (PER; rate of change of contrast intensity from baseline to peak intensity; in arbitrary units per second [a.u. /sec]) and area under the curve or blood volume (AUC; sum of contrast agent intensity from baseline to washout; in [a.u.]). The 3D parametric volumes were also broken down into the central, peripheral and the ratio of these two regions for diagnostic analysis. Generation of vascular heterogeneity and the 3D parametric volumes were based on image processing algorithms that were previously published³¹.

Data Analysis

Statistical analyses were performed using SPSS 20 (IBM Corporation, Armonk, NY) for *t*-tests and ANOVA and Stata ver. 15.1 (StataCorp LLC, College Station, TX) for ROC and regression analyses. Comparisons between TIC parameters obtained from malignant and benign lesions were performed using an unpaired *t*-test with a *p*-value of 0.05 or lower being

considered statistically significant. When comparing three or more independent groups a one-way ANOVA was applied. ROC analysis and reverse, step-wise logistical regression were used to assess diagnostic accuracy (for individual vascular parameters and in combination with each other) with histopathological biopsy results as the reference standard.

Results

Upon study completion, 236 patients had been enrolled and out of those image data were available for 219 cases. Among the 17 cases that had to be excluded, we were unable to gain peripheral venous access for contrast injection in 8 subjects, and 9 cases were incomplete due to a technical failure of the ultrasound scanner. The average age of the women who participated in this study was 52 ± 13 years. Biopsy results showed the study group consisted of 164 benign (75%) and 55 malignant lesions (25%), which was consistent with the clinical expectancy of ~80% of biopsies resulting in a benign finding. Furthermore, there was a statistically significant difference between the average age of patients with a malignant lesion (56 ± 11 years) compared to those with a benign lesion (49 ± 12 years), $p = 0.0027$.

When considering lesion sub-types, invasive ductal carcinomas (IDCs) made up the majority of the malignant cases (42/55, 78%), while fibroadenomas (FA) were the most frequent type (51/164, 31%) among the benign lesions. Other types of malignant lesions included, invasive lobular carcinoma, invasive papillary carcinoma and ductal carcinoma *in situ*, while, benign lesions included cysts, hyperplasia, lymph nodes, fat and other benign components. A total of 93 lesions (69 benign and 24 malignant) demonstrated vascular activity based on their PDI images. In terms of contrast imaging based on 3D SHI, 83 lesions (58 benign and 25 malignant) demonstrated vascular activity. Surprisingly, 3D HI showed only 8 lesions with vascularity (5 benign and 3 malignant). Statistically, 3D SHI performed significantly better than 3D HI in detecting lesion vascularity ($p < 0.0001$) Lesion subtypes and the ability to visualize vascularity with each of the imaging modes are listed in Table 2. Given the poor performance and small number of 3D HI cases identified with vascularity, no additional image processing and analysis was performed on this contrast imaging subset. Comparing the performance of 3D SHI and PDI in identifying lesions with vascularity showed no significant difference (83 vs. 93, respectively; $p = 0.52$) between the two modes. The average lesion cross-sectional area (based on measurements made in the largest cross-section of the lesion in the transverse plane) was greater for malignant lesions ($190.1 \pm 35.7 \text{ mm}^2$) compared to benign lesions ($124.1 \pm 15.5 \text{ mm}^2$). However, this was not a statistically significant finding ($p = 0.095$). Similarly, when considering only the vascular lesions, malignant lesions ($255.5 \pm 62.3 \text{ mm}^2$) were on average larger than the benign ones ($168.5 \pm 27.82 \text{ mm}^2$), but this was not a statistically significant difference either ($p = 0.215$).

4D View provided the ability to view and manipulate lesion volumes in a three-dimensional space for identifying regions of vascularity. The 3D TIC volumes of UCA flow were constructed after selection of an ROI corresponding to the vascular activity. Figure 2a and 2b shows a TIC volume generated from an IDC The wash-in and wash-out of the UCA are visible. Breathing motion artifacts and background tissue signal were suppressed to a large

extent by the smoothing filter and background template subtraction, as seen in Figure 2c and 2d.

The average T_s for malignant lesions was 19.9 ± 1.2 seconds and for benign lesions it was 18.7 ± 0.7 seconds. Likewise, the average TTP for malignant and benign lesions were 7.6 ± 2.3 seconds and 7.6 ± 2.6 seconds, respectively. Finally, malignant and benign lesions showed similar average TT's (27.9 ± 2.7 seconds vs. 23.9 ± 1.6 seconds). None of these differences were statistically significant ($p > 0.2$). However, when the most common malignant and benign lesion types (IDC and FA, respectively) were compared their average TTs were significantly different (28.9 ± 3.2 seconds vs. 20.9 ± 2.2 seconds; $p = 0.04$).

Similar to our previously described results,³¹ vascular heterogeneity in this enlarged sample size showed benign lesions the central zone to have significantly increased vascular activity relative the peripheral sections (1.83 ± 0.16 vs. 1.15 ± 0.09 dB; $p = 0.0003$). For malignant lesions, however, there was no significant difference in the vascular activity between the central and peripheral zones (1.72 ± 0.33 vs. 1.26 ± 0.21 dB; $p = 0.23$) indicative of an increased spread in vascularity within the cancers, which is consistent with the heterogeneous nature of malignant lesions^{39,40}.

Parametric volumes were generated based on the PER and AUC metrics. By creating 2D maps of vascular dynamics in the individual slices in the lesion volume, it was possible to wholly appreciate the global vascular behavior in each lesion. For example, the IDC shown in Figure 3a and 3b demonstrates the spread of vascularity within the central lesion area as well as in the peripheral zones. There seems to be spread of vascularity within the lesion area with a singular feeding vessel that is noticeable around the lesion periphery. Conversely, the ductal epithelium lined cyst in Figure 3c and 3d, exhibits vascularity that is confined to individual vessels that are well defined and structured. The majority of the lesion area appears hypoechoic void of any UCA flow as expected with most cystic lesions.

Both PER and AUC parametric maps provided insight into vascular dynamics in the individual slices of the 3D volume. However, compared to the PER maps, the AUC maps had noticeably increased image noise, due to motion artifacts experienced over the longer imaging period (including both wash-in and wash-out cf., Fig 3a and 3b).

Finally, the ability to characterize these breast lesions based on the vascular heterogeneity, PER or AUC parametric maps were determined by generating individual ROC curves based on each of these metrics in the central and peripheral zones of the lesion as well as a ratio of these two regions with the biopsy results as the reference standard (examples in Fig 4). The diagnostic accuracies (in the form of the area under the ROC curve; A_z) for each of the quantitative SHI metrics ranged from minimally better than chance at 0.52 to a reasonable 0.75 (see Table 3). To determine the optimal combination of metrics for characterization, a reverse, step-wise logistical regression model was constructed. Based on this model, the optimal combination of parameters were the vascular heterogeneity ratio combined with PER and AUC in the central zone, which achieved an A_z of 0.90 (cf., Fig 4)

Discussion

In this study, we explored the use of 3D contrast-enhanced ultrasound to perform HI and SHI to visualize, quantify and characterize breast lesions based on their vascular characteristics. 3D SHI was considerably better at detecting vascular flow in the lesions compared to 3D HI (83 cases in SHI vs. 8 cases in HI, $p < 0.0001$). The vascular detection rate for 3D SHI was comparable with PDI ($n = 93$) with no significant difference in performance between these two groups ($p = 0.52$). The poor performance of 3D HI with less than 5% of the total 3D HI lesion volumes showing any signs of UCA was an unexpected finding. The increased tissue suppression in 3D SHI might be the reason for its marked improvement over 3D HI in visualizing lesion vascularity. Additionally, a weaker signal response from the microbubbles, due to insufficient acoustic output, lower overall dosage, and an overall reduced sensitivity of the transducer could have impacted the visualization of UCA on 3D HI. It is also important to note that there was up to a 5-fold increase in the contrast dose for 3D SHI in some cases based on the patient weight compared to the dosing for 3D HI, which was fixed for all patients. These dosages were selected based on previously reported work^{34,41}, although it must be noted that our dosage selection was based on *in vitro* flow phantom, animal studies for kidney imaging and a clinical breast imaging study that utilized a 2D linear transducer on a different ultrasound system. In these cases, either the combination of an ideal phantom or a large vascular organ (i.e., kidney) in the animal studies these dosages were optimal for 3D HI and 3D SHI. However, these dosages, more so for 3D HI were suboptimal for breast lesion imaging in humans. Additionally, this study was conducted under an FDA approved IND with a stipulation to limit dosing to a single vial (1.5 mL) of Definity per patient which further limited our ability to modify dosages for each imaging mode. Since the focus of this study was primarily on 3D SHI, the dosing scheme was not changed during the course of the study. However, future studies using 3D HI may require scaling of dosages based on weight (similar to 3D SHI) in order to improve contrast visualization.

Quantitative analysis of vascular heterogeneity using the change in UCA signal intensity from baseline to peak for each 2D image slice in the lesion volume showed a uniform distribution of vascular signal in the central sections of the benign lesions (possibly from larger central vessels) and minimal activity in the peripheral zone and this distinct characteristic was found to be significantly different ($p = 0.0003$). In malignant lesions however, a wider distribution of vascular signal was observed in the central and peripheral regions of the lesion resulting in no significant differences in vascularity ($p = 0.24$). Previously, our group reported findings based on an initial data set of 138 patients³¹. This included evaluation of the vascular heterogeneity in 68 lesions (19 malignant and 49 benign), where a similar finding of significantly increased vascular activity in the central vs. the peripheral zones in the benign lesions ($p < 0.001$) and dispersed vascular activity throughout the lesion in the malignant lesions ($p = 0.24$) was found. However, in that study, the ratio of vascular activity (between the central and peripheral zones) and the use of parametric maps to evaluate PER and AUC of the UCA flow within the lesions to subsequently determine the diagnostic accuracy of using these parameters to characterize the lesions was not performed. Here, parametric maps based on PER and AUC highlighted the

variations in the vascular kinetics for individual voxels in the lesion volume. It was observed that for malignant cases, specifically for IDC's the vascularity was dispersed throughout the lesion volume with feeding vessels around the lesion boundary. Benign cases demonstrated a more structured vasculature, usually with a large well defined vessel(s) within the lesion volume. This behavior was consistent across both the vascular heterogeneity plots as well as 3D parametric volumes.

A significantly higher TT was observed in IDC compared to FA (28.9 ± 13.9 vs. 20.9 ± 11.1 seconds respectively, $p = 0.04$). This finding is important given what is known about the tumor vascularity, especially in aggressive malignant lesions such as IDCs. Often in these types of lesions there are altered vascular patterns made up of leaky vessels and increased shunting that could contribute towards an increased circulation time of UCA within the tumor volume. This in turn increases the overall TT in these malignant lesions compared to the more structured vasculature and therefore shorter TT in benign lesions. Early work involving angiography of breast carcinomas demonstrated chaotic vascular patterns including abnormal feeding vessels and leaky vasculature^{42,43}. A separate study of endothelial cell proliferation (an essential precursor to angiogenesis) in breast lesions,³⁹ showed a predominant presence at the periphery for tumors. Work done by Weidner et al.⁴⁰, involving the microvessel density in invasive breast cancer concluded that the tumors were frequently heterogeneous in their microvessel density and that the areas of high neovascularization could occur anywhere in the tumor. Recently, Chen et al.⁴⁴ showed significant difference in peripheral vessel characteristics between benign and malignant breast lesions using 3D CEUS. The results of this study are consistent with the vascular characteristics (i.e., parameters associated with the angiogenic vessels 20 to 40 μm in diameter⁴⁵) and behavior expected in these malignant breast lesions and further establishes both CEUS and 3D US imaging as tools to evaluate these structural and functional features.

Finally, nine quantitative contrast enhanced vascularity measures that included the central, peripheral and their ratio for vascular heterogeneity, PER distribution and AUC distribution were investigated for breast lesion characterization using biopsy results as the reference standard. Although the individual accuracies of these metrics to characterize breast lesions were quite low ($< 76\%$), the optimal logistical regression model achieved an excellent diagnostic accuracy of 90%. Similar findings using CEUS for breast lesion characterization in clinical studies have been independently reported by other groups, A_z : range 0.84 to 0.95, sensitivity: range 0.85 to 0.92 and specificity: range 0.81 to 0.89⁴⁶⁻⁵⁰ with the optimal model reaching an A_z of 0.953, sensitivity of 98.9% and specificity of 58.2% for BI-RADS-US + CEUS⁴⁸.

It is important to consider the limitations of this study. First, in terms of lesions vascularity, 50% of the total IDC's that were included in this study did not show any signs of vascularity (both on 3D SHI and PDI) and therefore were not characterized using 3D SHI. It is certainly possible for malignant lesions to become necrotic over a period of time and not sustain any active vascularity within the lesion itself. In such a scenario characterization using this technique would not be possible. Furthermore, it is also possible that there could be increased vascularity in the immediate area surrounding such lesions to maintain growth and progression^{39,51,52} in both lesions that maintained active vascularity within the lesion itself

or those with a necrotic core. By imaging the surrounding area of the lesion, these vascular features could be included in the lesion assessment. However, the 3D volume acquisition rate is directly linked to the size of the imaging area. Increasing the image area to include both the lesion and surrounding area would require lowering the volume acquisition rates (below 2 volumes per second), which might compromise capturing the UCA kinetics. Similarly, in order to acquire the full lesion volume at higher acquisition rates, the raw image data is saved at a low resolution (usually around 40×50 pixels per 2D image slice). This significantly lowers the image definition of the structures in the acquired image. In a previous study the use of a dynamic cumulative maximum intensity technique (CMI) combined with 2D SHI was explored and achieved an A_z of 0.90 for breast lesion characterization³³. Although theoretically possible, the translation of this technique to 3D imaging is yet to be explored. The CMI algorithm uses a template matching algorithm to compensate for motion in order accurately create CMI images. This would be computationally less expensive to perform for 2D than 3D. However, given the possible benefits for improving the diagnostic accuracy this should certainly be explored and, with advances in transducer technology and the development of matrix arrays for 3D imaging these limitations could be overcome in future studies. Although modified to perform 3D SHI, the inherent overall reduced sensitivity of the probe and lower dose contributed to the few number of lesions with contrast enhancement being detected in 3D HI and a lower number of cases with enhancement in 3D SHI compared to visualization of vascularity with PDI.

During data acquisition, imaging parameters were optimized on a case-by-case basis making cross comparisons challenging. However, this individual optimization was performed in order to achieve the best possible image data for each patient. The end goal of this clinical study was to provide useful diagnostic information as an adjunct to mammography in order to deliver a better diagnostic assessment for the patient. Finally, while biopsies were performed on all lesions as the reference standard, no independent information about the lesion vascularity was available to compare with the 3D SHI and PDI results.

To conclude, in this study, the use of 3D contrast-enhanced nonlinear ultrasound imaging, specifically 3D SHI for visualizing, quantifying vascularity and subsequently characterizing breast lesions was evaluated. Our results showed that 3D SHI is able to detect UCA flow in vascular breast lesions. Significant differences were identified in the distribution of vascularity across the lesion volume between the malignant and benign lesions and these differences were quantified. Finally, 3D SHI appears to be able to accurately characterize vascular breast lesions by employing a combination of quantitative parameters (with A_z reaching 0.90). Evaluation of such quantitative CEUS parameters may aid in the characterization of breast lesions by providing an accurate, cost-effective and patient friendly imaging tool for diagnosis of breast lesions.

Acknowledgments

Funding and Drug support: This work was supported by National Institutes of Health Grant R01 CA140338, U.S. Army Medical Research Materiel Command Grant W81XWH-11-1-0630 and Lantheus Medical Imaging supplied Definity™.

Appendix

Inclusion criteria

1. Be a female diagnosed by x-ray mammography and/or grayscale US (performed within 90 days prior to study procedure) as having a solid breast mass or abnormal area without a mass.
2. Be scheduled for a biopsy (core/excisional/lumpectomy) of mass or region of abnormality or for mastectomy within 30 days after this study procedure.
3. Be at least 21 years of age.
4. Be medically stable.
5. Must have a negative pregnancy test if a female of child-bearing potential.

Exclusion criteria

1. Patients who are pregnant or nursing.
2. Patients whose breast lesion is unequivocally a cyst by unenhanced US.
3. Patients currently on chemotherapy or with other primary cancers requiring systemic treatment
4. Patients who are medically unstable, seriously or terminally ill whose clinical course is unpredictable.
5. Patients with clinically unstable cardiac arrhythmias (recurrent ventricular tachycardia), uncontrolled congestive heart failure, recent cerebral hemorrhage.
6. Patients with known hypersensitivity to perflutren.
7. Patients with cardiac shunts, congenital heart defects, severe emphysema, pulmonary vasculitis, or history of pulmonary emboli.
8. Patients who have had excisional biopsy/lumpectomy of the current area of interest within the past 6 weeks.

References

1. Siegel RL, Miller KD, Jemal A. Cancer statistics, 2018. *CA Cancer J Clin.* 2018;68(1):7–30. [PubMed: 29313949]
2. Kopans DB. *Breast Imaging.* 3rd ed. Philadelphia, PA: Lippincott Williams & Wilkins; 2007.
3. Zonderland HM, Coerkamp EG, Hermans J, et al. Diagnosis of Breast Cancer: Contribution of US as an Adjunct to Mammography. *Radiology.* 1999;2(213):413–422.
4. Yankaskas BC, Haneuse S, Kapp JM, et al. Performance of first mammography examination in women younger than 40 years. *J Natl Cancer Inst.* 2010;102(10):692–701. [PubMed: 20439838]
5. Yankaskas BC, Taplin SH, Ichikawa L, et al. Association between Mammography Timing and Measures of Screening Performance in the United States. *Radiology.* 2005;234(2):363–373. [PubMed: 15670994]
6. McDonald DM, Choyke PL. Imaging of angiogenesis: From microscope to clinic. *Nat Med.* 2003;9:713–725. [PubMed: 12778170]

7. Li WW. Tumor angiogenesis: Molecular pathology, therapeutic targeting, and imaging. *Acad Radiol.* 2000;7(10):800–811. [PubMed: 11048878]
8. Jain RK. Delivery of novel therapeutic agents in tumors: Physiological barriers and strategies. *J Natl Cancer Inst.* 1989;81(8):570–576. [PubMed: 2649688]
9. Stavros AT, Thickman D, Rapp CL, et al. Solid breast nodules: use of sonography to distinguish between benign and malignant lesions. *Radiology.* 1995;196(1):123–124. [PubMed: 7784555]
10. Taylor KJW, Merritt C, Piccoli C, et al. Ultrasound as a complement to mammography and breast examination to characterize breast masses. *Ultrasound Med Biol.* 2002;28(1):19–26. [PubMed: 11879948]
11. Adler DD, Carson PL, Rubin JM, et al. Doppler ultrasound color flow imaging in the study of breast cancer: Preliminary findings. *Ultrasound Med Biol.* 1990;16(6):553–559. [PubMed: 2238263]
12. Carson PL, Fowlkes JB, Roubidoux MA, et al. 3-D color Doppler image quantification of breast masses. *Ultrasound Med Biol.* 1998;24(7):945–952. [PubMed: 9809628]
13. Ferrara KW, Merritt CRB, Burns PN, et al. Evaluation of tumor angiogenesis with US: Imaging, Doppler, and contrast agents. *Acad Radiol.* 2000;7(10):824–839. [PubMed: 11048880]
14. Xiao X, Chen X, Guan X, et al. Superb microvascular imaging in diagnosis of breast lesions: a comparative study with contrast-enhanced ultrasonographic microvascular imaging. *Br J Radiol.* 2016;89(1066):1–8.
15. Ma Y, Li G, Li J, et al. The Diagnostic Value of Superb Microvascular Imaging (SMI) in Detecting Blood Flow Signals of Breast Lesions: A Preliminary Study Comparing SMI to Color Doppler Flow Imaging. *Medicine (Baltimore).* 2015;94(36):e1502–1507. [PubMed: 26356718]
16. Machado P, Segal S, Lyschik A, et al. A novel microvascular flow technique: Initial results in thyroids. *Ultrasound Q.* 2016;32(1):67–74. [PubMed: 25900162]
17. Goldberg BB, Raichlen JS, Forsberg F. *Ultrasound Contrast Agents : Basic Principles and Clinical Applications.* 2nd ed. London: Martin Dunitz; 2001.
18. Forsberg F. *Physics of ultrasound contrast agents* In: *Ultrasound Contrast Agents.* London, UK: Martin-Dunitz; 1996:9–20.
19. Burns PN, Powers JE, Simpson DH, et al. Harmonic power mode Doppler using microbubble contrast agents: an improved method for small vessel flow imaging. *Proc IEEE Ultrason Symp.* 1994;3:1547–1550.
20. Goertz DE, Frijlink ME, de Jong N, et al. Nonlinear intravascular ultrasound contrast imaging. *Ultrasound Med Biol.* 2006;32(4):491–502. [PubMed: 16616596]
21. Forsberg F, Shi WT, Goldberg BB. Subharmonic imaging of contrast agents. *Ultrasonics.* 2000;38(1):93–98. [PubMed: 10829636]
22. de Jong N, Emmer M, van Wamel A, et al. Ultrasonic characterization of ultrasound contrast agents. *Med Biol Eng Comput.* 2009;47(8):861–873. [PubMed: 19468770]
23. Leighton TG, Apfel RE. The Acoustic Bubble. *J Acoust Soc Am.* 1994;96(4):2616.
24. Eisenbrey JR, Forsberg F. Contrast-enhanced ultrasound for molecular imaging of angiogenesis. *Eur J Nucl Med Mol Imaging.* 2010;37(S1):138–146.
25. Hamilton MF, Blackstock DT. *Nonlinear Acoustics.* San Diego, CA: Academic Press; 1998.
26. Kedar RP, Cosgrove D, McCready VR, et al. Microbubble contrast agent for color Doppler US: effect on breast masses. *Work in progress. Radiology.* 1996;198(3):679–686. [PubMed: 8628854]
27. Madjar H, Prömpeler HJ, Del Favero C, et al. A new Doppler signal enhancing agent for flow assessment in breast lesions. *Eur J Ultrasound.* 2000;12(2):123–130. [PubMed: 11118919]
28. Yang WT, Tse GMK, Lam PKW, et al. Correlation between color power Doppler sonographic measurement of breast tumor vasculature and immunohistochemical analysis of microvessel density for the quantitation of angiogenesis. *J Ultrasound Med.* 2002;21(11):1227–1235. [PubMed: 12418764]
29. Zdemir A, Kilic K, Ozdemir H, et al. Contrast-enhanced power Doppler sonography in breast lesions: effect on differential diagnosis after mammography and gray scale sonography. *J Ultrasound Med.* 2004;23(2):183–187. [PubMed: 14992355]

30. Stuhmann M, Aronius R, Schietzel M. Tumor vascularity of breast lesions: Potentials and limits of contrast-enhanced Doppler sonography. *Am J Roentgenol.* 2000;175(6):1585–1589. [PubMed: 11090380]
31. Sridharan A, Eisenbrey JR, MacHado P, et al. Quantitative analysis of vascular heterogeneity in breast lesions using contrast-enhanced 3-D harmonic and subharmonic ultrasound imaging. *IEEE Trans Ultrason Ferroelectr Freq Control.* 2015;62(3):502–510. [PubMed: 25935933]
32. Forsberg F, Piccoli CW, Merton DA, et al. Breast Lesions: Imaging with Contrast-enhanced Subharmonic US—Initial Experience. *Radiology.* 2007;244(3):718–726. [PubMed: 17690324]
33. Dave JK, Forsberg F, Fernandes S, et al. Static and dynamic cumulative maximum intensity display mode for subharmonic breast imaging: A comparative study with mammographic and conventional ultrasound techniques. *J Ultrasound Med.* 2010;29(8):1177–1185. [PubMed: 20660451]
34. Eisenbrey JR, Sridharan A, Machado P, et al. Three-dimensional subharmonic ultrasound imaging in vitro and in vivo. *Acad Radiol.* 2012;19(6):732–739. [PubMed: 22464198]
35. Kitzman DW, Goldman ME, Gillam LD, et al. Efficacy and safety of the novel ultrasound contrast agent perflutren (definity) in patients with suboptimal baseline left ventricular echocardiographic images. *Am J Cardiol.* 2000;86(6):669–674. [PubMed: 10980221]
36. Goertz DE, de Jong N, van der Steen AFW. Attenuation and Size Distribution Measurements of Definity™ and Manipulated Definity™ Populations. *Ultrasound Med Biol.* 2007;33(9):1376–1388. [PubMed: 17521801]
37. Sridharan A, Eisenbrey JR, Liu J-B, et al. Perfusion estimation using contrast-enhanced 3-Dimensional subharmonic ultrasound imaging: An in vivo study. *Invest Radiol.* 2013;48(9):654–660. [PubMed: 23695085]
38. Eisenbrey JR, Daecher A, Kramer MR, et al. Effects of needle and catheter size on commercially available ultrasound contrast agents. *J Ultrasound Med.* 2015;34(11):1961–1968. [PubMed: 26384606]
39. Fox SB, Gatter KC, Bicknell R, et al. Relationship of Endothelial Cell Proliferation to Tumor Vascularity in Human Breast Cancer. *Cancer Res.* 1993;53(18):4161–4163. [PubMed: 7689928]
40. Weidner N, Folkman J, Pozza F, et al. Tumor angiogenesis: A new significant and independent prognostic indicator in early-stage breast carcinoma. *J Natl Cancer Inst.* 1992;84(24):1875–1887. [PubMed: 1281237]
41. Hoyt K, Umphrey H, Lockhart M, et al. Ultrasound Imaging of Breast Tumor Perfusion and Neovascular Morphology. *Ultrasound Med Biol.* 2015;41(9):2292–2302. [PubMed: 26116159]
42. Feldman F. Angiography of cancer of the breast. *Cancer.* 1969;23(4):803–808. [PubMed: 5775969]
43. Watt AC, Ackerman LV, Shetty PC, et al. Differentiation between benign and malignant disease of the breast using digital subtraction angiography of the breast. *Cancer.* 1985;56(6):1287–1292. [PubMed: 3896454]
44. Chen M, Wang WP, Jia WR, et al. Three-dimensional contrast-enhanced sonography in the assessment of breast tumor angiogenesis correlation with microvessel density and vascular endothelial growth factor expression. *J Ultrasound Med.* 2014;33(5):835–846. [PubMed: 24764339]
45. Forsberg F, Kuruvilla B, Pascua MB, et al. Comparing Contrast-Enhanced Color Flow Imaging and Pathological Measures of Breast Lesion Vascularity. *Ultrasound Med Biol.* 2008;34(9):1365–1372. [PubMed: 18436369]
46. Huang R, Jiang L, Xu Y, et al. Comparative Diagnostic Accuracy of Contrast-Enhanced Ultrasound and Shear Wave Elastography in Differentiating Benign and Malignant Lesions: A Network Meta-Analysis. *Front Oncol.* 2019;9:102–121. [PubMed: 30891425]
47. Miyamoto Y, Ito T, Takada E, et al. Efficacy of Sonazoid (perflubutane) for contrast-enhanced ultrasound in the differentiation of focal breast lesions: Phase 3 multicenter clinical trial. *Am J Roentgenol.* 2014;202(4):W400–W407. [PubMed: 24660739]
48. Xiao X, Jiang Q, Wu H, et al. Diagnosis of sub-centimetre breast lesions: combining BI-RADS-US with strain elastography and contrast-enhanced ultrasound—a preliminary study in China. *Eur Radiol.* 2017;27(6):2443–2450. [PubMed: 27761708]
49. Yuan Z, Quan J, Yunxiao Z, et al. Diagnostic value of contrast-enhanced ultrasound parametric imaging in breast tumors. *J Breast Cancer.* 2013;16(2):208–213. [PubMed: 23843855]

50. Xia HS, Wang X, Ding H, et al. Papillary breast lesions on contrast-enhanced ultrasound: morphological enhancement patterns and diagnostic strategy. *Eur Radiol.* 2014;24(12):3178–3190. [PubMed: 25149297]
51. Lee SW, Choi HY, Baek SY, et al. Role of color and power Doppler imaging in differentiating between malignant and benign solid breast masses. *J Clin Ultrasound.* 2002;30(8):459–464. [PubMed: 12242733]
52. Raza S, Baum JK. Solid breast lesions: evaluation with power Doppler US. *Radiology.* 1997;203(1):164–168. [PubMed: 9122386]

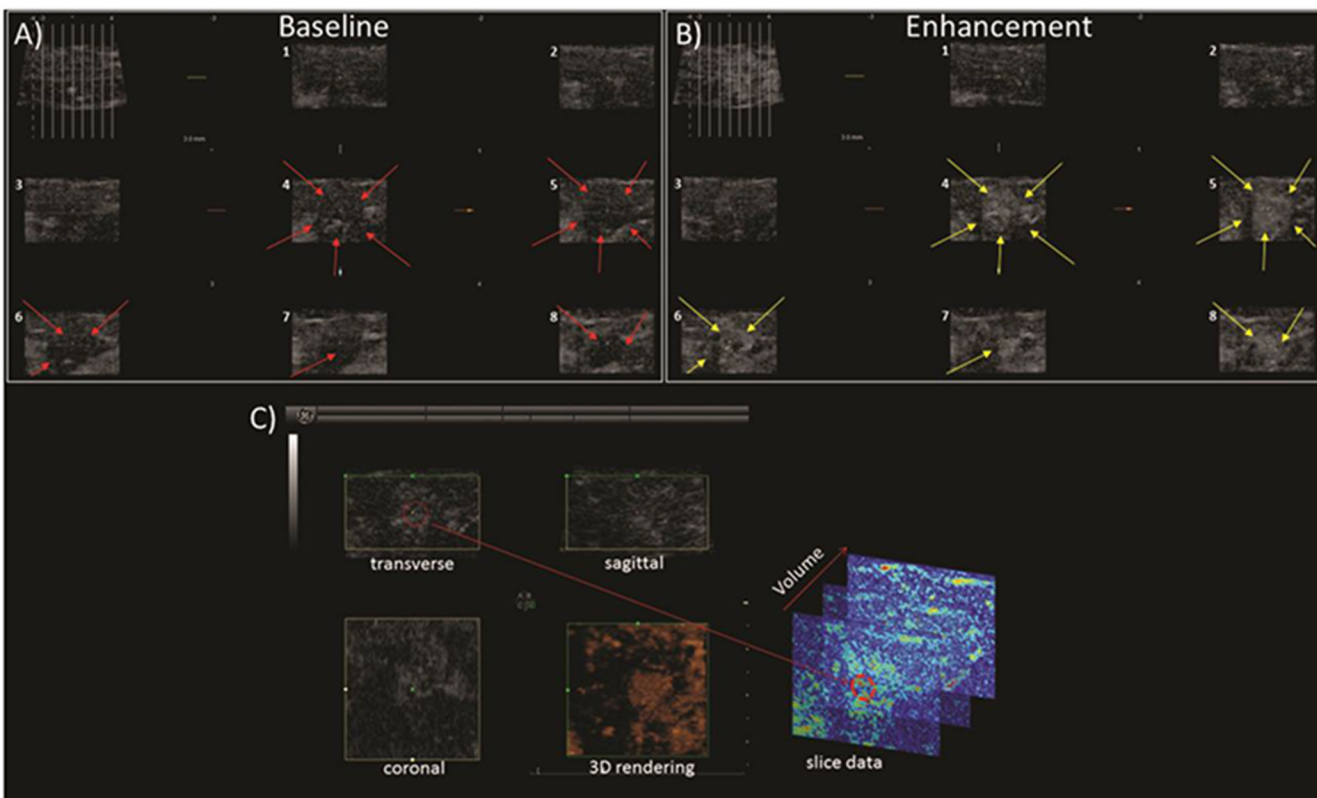


Figure 1. The capability of 4DView to perform slicing through the lesion volume and selection of ROI. A) Baseline lesion volume of an invasive ductal carcinoma is presented as a series of individual slices. The lesion area (denoted by the red arrows) void of contrast enhancement is seen in slices 4-8. B) The same lesion volume and its corresponding slices are seen during the enhancement phase. Contrast-enhancement is visualized (yellow arrows) within the lesion volume and can be seen in the individual slices 4-8. In this case each slice was separated by 3 mm. C) Visualization of the lesion with contrast enhancement using 4DView (3-axes plus the 3D rendered image is seen). An ROI (red dashed circle) selected in the transverse axis is mapped to the raw slice data that is extracted in MATLAB for post-processing.

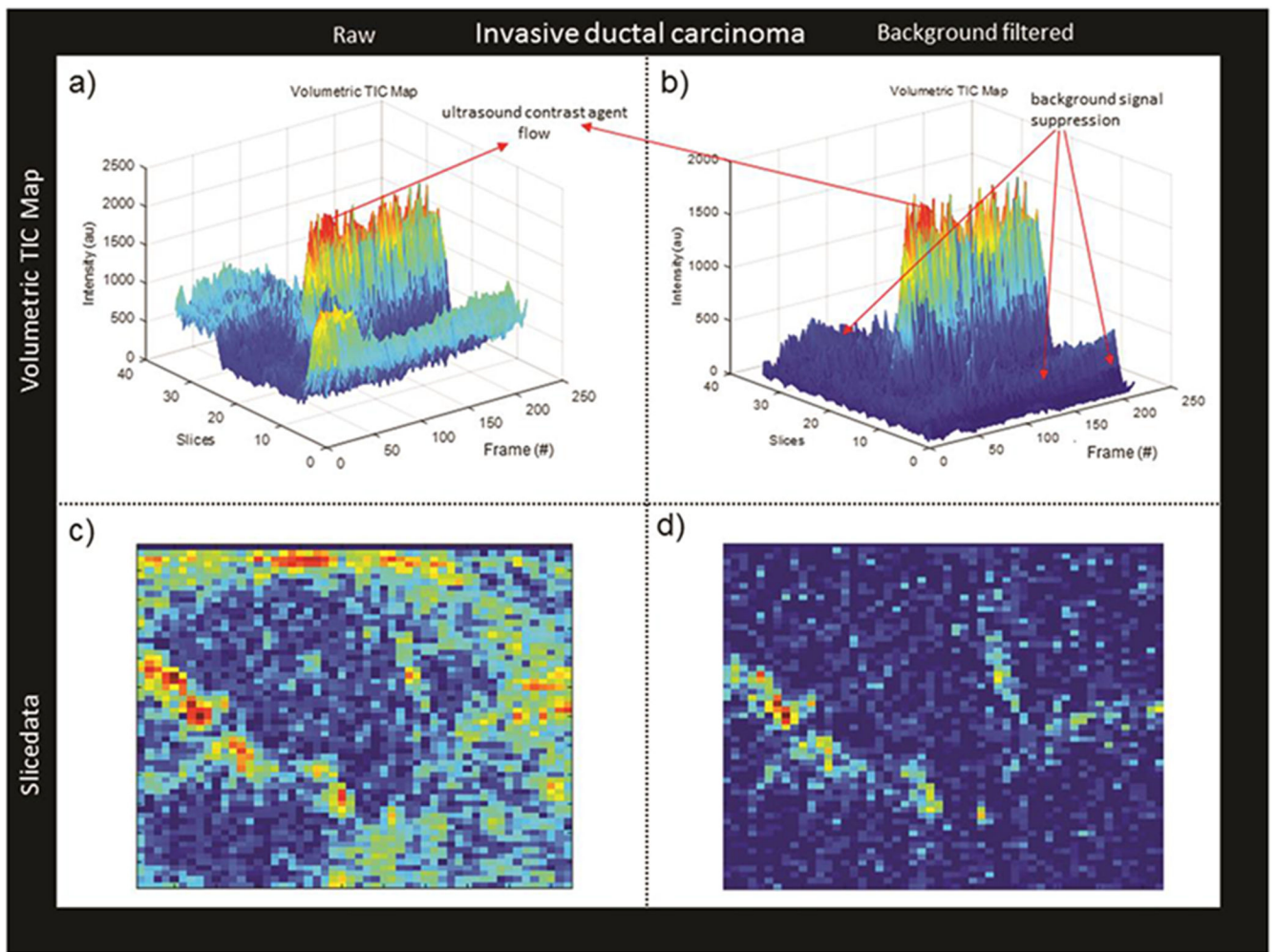


Figure 2. The 3D TIC volume generated from an invasive ductal carcinoma (a) before background filtering and (b) after background filtering. An individual slice corresponding to the same lesion from the (c) raw slicedata and (d) after background filtering is also shown.

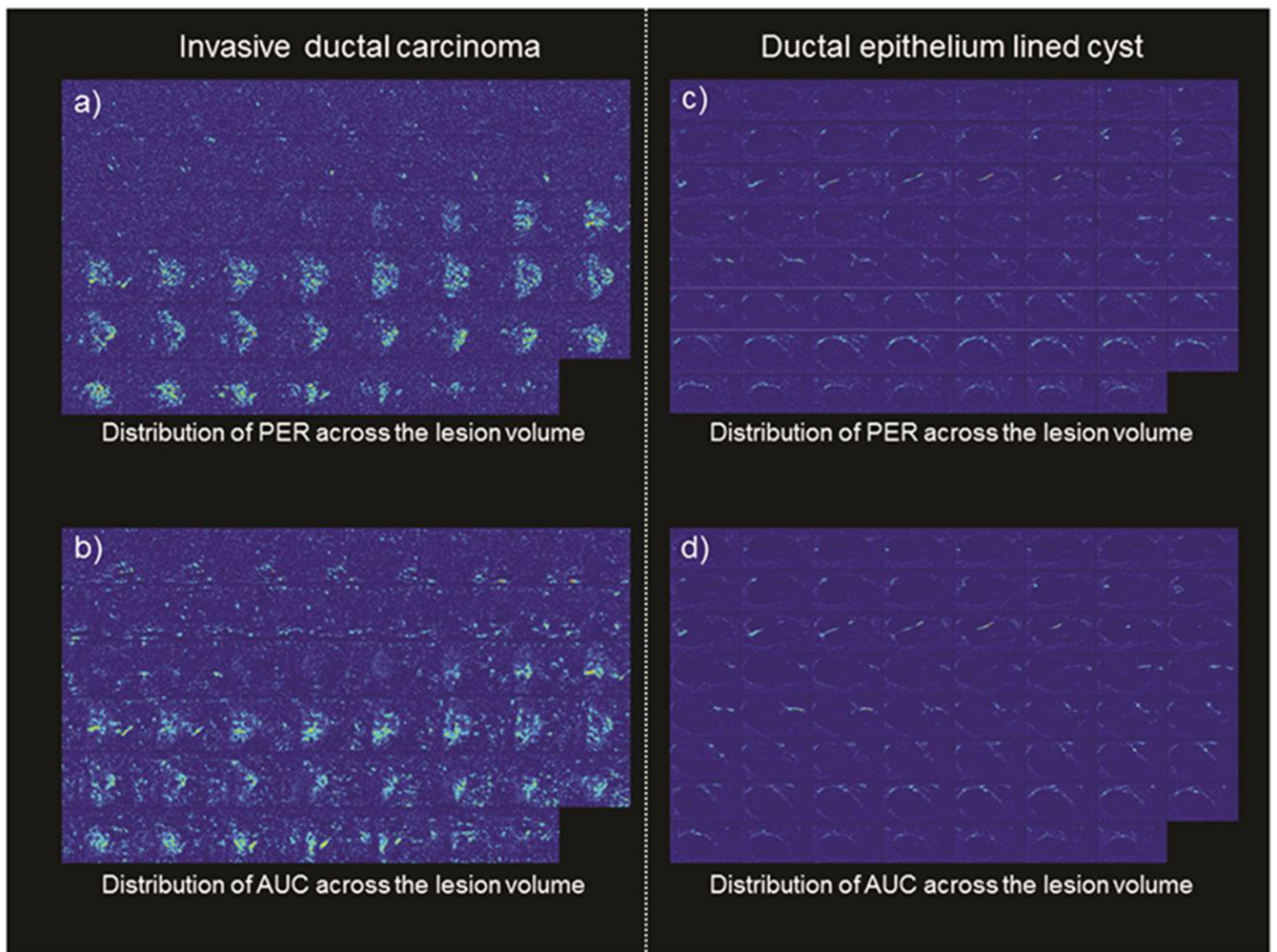


Figure 3.

The distribution of vascularity across the lesion volume is shown as a montage of sliced data for (a) PER in an invasive ductal carcinoma (IDC) (b) AUC in an IDC (c) PER in a ductal epithelium lined cyst and (d) AUC in a ductal epithelium lined cyst. For the IDC the spread of vascularity is seen across the central and peripheral lesion areas while in the ductal epithelium lined cyst the vascularity is confined to individual vessels that are well defined and structured.

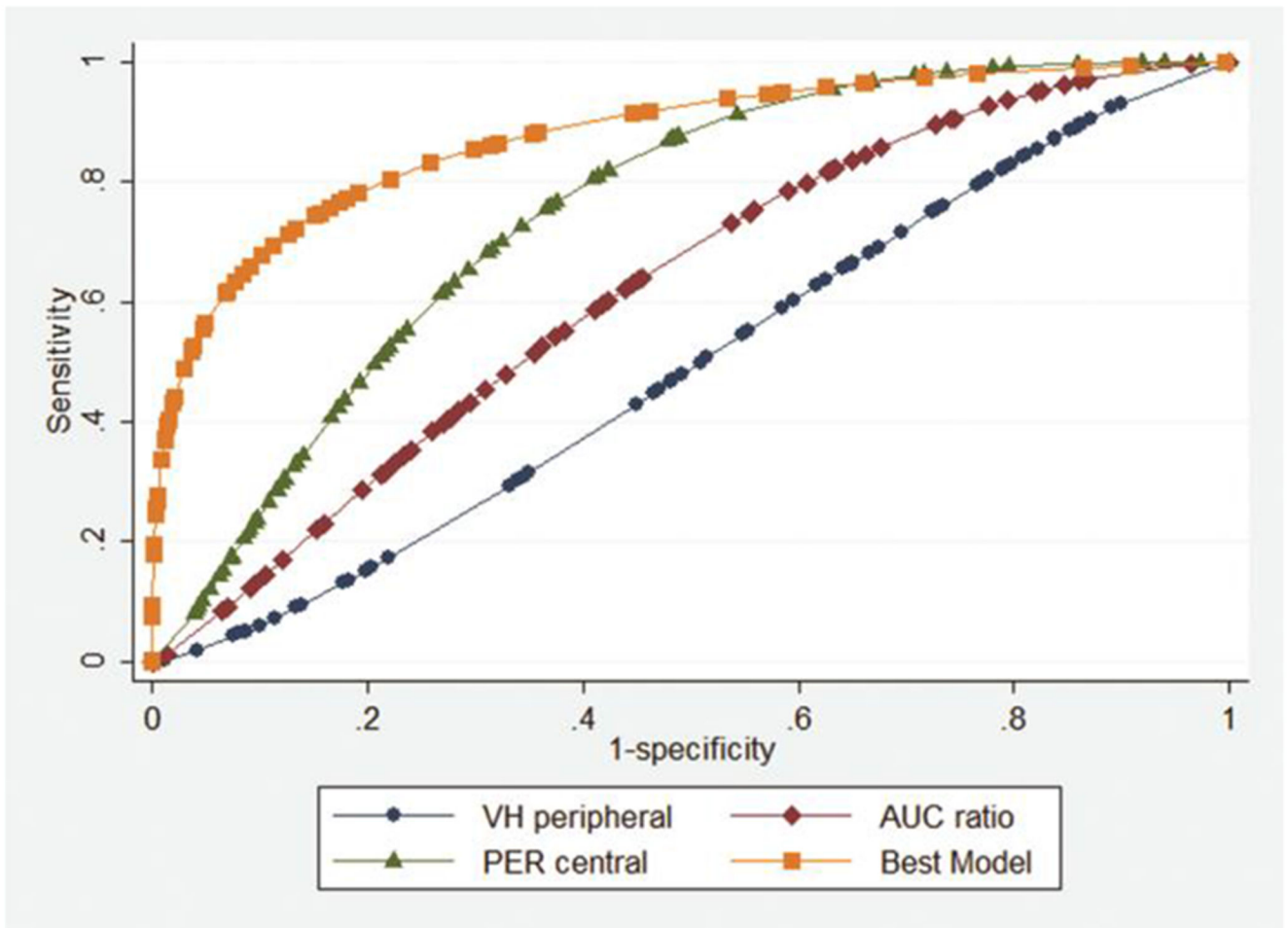


Figure 4. ROC curves for vascular heterogeneity (VH) in the peripheral ROI ($A_z = 0.52$; in blue); PER in the central ROI ($A_z = 0.69$; in green); AUC ratio ($A_z = 0.70$; in red) and the best regression model ($A_z = 0.90$; in orange).

Table 1.

List of time-points perfusion measures generated from the 3D TIC volumes based on UCA¹ flow within the lesion.

TIC metric	Description
T _S (sec ²)	Wash-in time: time point corresponding to the arrival UCA flow in the lesion
T _B (sec)	Baseline time: time point corresponding to 10% of peak UCA intensity along the TIC wash-in
T _P (sec)	Peak time: time point of peak UCA intensity
T _W (sec)	Wash-out time: time point of return to baseline UCA intensity along the TIC wash-out
TTP (sec)	Time-to-peak: time from baseline (T _B) to peak (T _P)
TT (sec)	Total transit time: time from baseline (T _B) to washout (T _W)
PER (a.u. ³ /sec)	Rate of change of UCA intensity from baseline (T _B) to peak (T _P)
AUC (a.u.)	Sum of UCA intensity from baseline (T _B) to wash-out (T _W)

¹ ultrasound contrast agent;

² seconds;

³ arbitrary units

Table 2.

Lesion subtypes including the number of lesions in each category and the number of cases with vascular visualization in PDI, 3D HI and 3D SHI.

Malignant type	No. of lesions	Vascular visualization (no. of cases)		
		PDI	3D HI	3D SHI
Invasive ductal carcinoma	42	18	3	21
Ductal carcinoma in situ	7	3	0	3
Invasive lobular carcinoma	4	0	0	1
Invasive papillary carcinoma	2	1	0	0
Total	55	22	3	25
Benign type				
Fibroadenoma	51	23	5	27
Cysts	31	0	0	5
Hyperplasia	22	13	0	6
Lymph node	14	3	0	1
Adenosis	8	4	0	4
Fat	4	0	0	1
Intraductal papilloma	3	4	0	8
Fibroepithelial lesion	2	1	0	1
Mastitis	2	0	0	0
Other	27	21	0	5
Total	164	69	5	58

Table 3.

The area under the ROC curve; Az for vascular heterogeneity, PER and AUC as a ratio (of central to peripheral regions) and in the central and peripheral regions separately are listed. The Az range from 0.52 to 0.75.

	Vascular Heterogeneity	PER	AUC
Ratio	0.73	0.66	0.70
Central	0.70	0.69	0.75
Peripheral	0.52	0.73	0.65